Steel and Composite Structures, *Vol. 27, No. 4 (2018) 417-426*
DOI: https://doi.org/10.12989/scs.2018.27.4.417

Seismic behaviors of ring beams joints of steel tube-reinforced concrete column structure

Yingying Zhang [*1], Jianing Pei [1], Yuan Huang [1], Ke Lei [2], Jie Song [1] and Qilin Zhang [3]

[1] *State Key Laboratory for Geomechanics and Deep Underground Engineering, Jiangsu Key Laboratory of Environmental Impact and Structural Safety in Engineering, China University of Mining and Technology, Xuzhou Jiangsu, 221116, China*
[2] *China Construction Eighth Engineering Divisions Corp. Ltd, Shanghai, 200135, China*
[3] *College of Civil Engineering, Tongji University, Shanghai, 200092, China*

(*Received November 21, 2017, Revised March 8, 2018, Accepted March 17, 2018*)

Abstract. This paper presents the seismic behaviors and restoring force model of ring beam joints of steel tube-reinforced concrete column structure under cyclic loading. First, the main failure mode, ultimate bearing capacity, stiffness degradation and energy dissipation capacity are studied. Then, the effects of concrete grade, steel grade, reinforcement ratio and radius-to-width ratios are discussed. Finally, the restoring force model is proposed. Results show that the ring beam joints of steel tube-reinforced concrete column structure performs good seismic performances. With concrete grade increasing, the ultimate bearing capacity and energy dissipation capacity increase, while the stiffness degradation rates increases slightly. When the radius-width ratio is 2, with reinforcement ratio increasing, the ultimate bearing capacity decreases. However, when the radius-to-width ratios are 3, with reinforcement ratio increasing, the ultimate bearing capacity increases. With radius-to-width ratios increasing, the ultimate bearing capacity decreases slightly and the stiffness degradation rate increases, but the energy dissipation capacity increases slightly.

Keywords: steel tube-reinforced concrete column structure; ring beam joints; seismic behaviors; restoring force model

1. Introduction

Recently, with development of economy and technology, high-rise buildings are widely welcomed in actual engineering. In high-rise buildings, the load of the bottom columns is always very high, and the “fat beam and big column” phenomenon can be easily observed (Nie 2011, Yu *et al*. 2013, Lee and Fenves 1998). The concrete filled steel tubular laminated column (abbreviated as CFSTLC), composed of concrete-filled steel tubular column and external reinforced concrete, is first proposed in China (Zhong 2003). Compared with traditional reinforced concrete columns, the middle steel tube can perform a better ductility. Compared with traditional concrete filled steel tube columns (abbreviated as CFSTC), the outer concrete can effectively reduce the corrosion of steel tube and delay the local buckling of steel tube.

Due to appearance of steel tube, the mechanical properties of inner and outer concrete both changes, because the constraint of steel tube makes the core concrete under a very complex state. The failure of the concrete may change from original brittle failure to possible plastic failure. Besides, the steel tube can also improve the strength and ductility of outer reinforced concrete. In addition, the inner and outer concrete may avoid or delay the local buckling of steel tube, as shown in Fig. 1. Then, the stress-strain relation of concrete is very different from the traditional concrete. Besides, the outer concrete outside can provide a better fire protection (CECS 2005).

In this paper, a project of commercial complex in Shanghai Xing Hui Center project is taken as a prototype. The paper is based on its material parameters and modeled by ABAQUS finite element software. The seismic performance of the ring beams joints of steel tube-reinforced concrete column structure under cyclic loading is simulated. The effects of concrete strength, steel and steel pipe strength, reinforcement ratio of steel bar and arrangement of steel bars on seismic behavior of the joints were studied. The law of stiffness degradation and energy dissipation capacity of the joints under repeated low-cycle loading are obtained, and the prediction of the seismic performance of similar nodes is made.

The ring beams joints of steel tube-reinforced concrete column structure cancels the hole in the steel pipe wall and solves the problem of stress concentration on the steel pipe. However, the addition of the ring beam changes the stress of the concrete and the steel bar in the core of the composite column. The radius-width ratio of the ring beam, the ratio of the reinforcement and the strength of the concrete all affect the seismic performance of the component. Therefore, it is necessary to study the seismic behavior of the ring-girder node.

There have been many experiments on the seismic behaviors of steel tube-reinforced concrete column structure, including axial compression ratio, ultimate load, ductility and energy dissipation. Wang (Wang *et al*. 2016)

∗Corresponding author, Professor,
E-mail: zhangyingying85@163.com

http://www.techno-press.org/?journal=scs&subpage=6
ISSN: 1229-9367 (Print), 1598-6233 (Online)

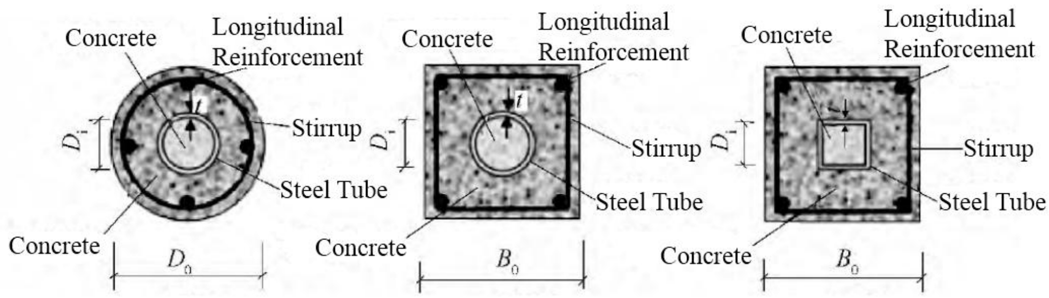

(a) Round-round (b) Rectangular-round (c) Rectangular-rectangular

Fig. 1 Cross sections of steel tube-reinforced concrete column structure

studied the eccentric compression of steel tube-reinforced concrete column structure and found that the ultimate state is peripheral compressive damage of outer concrete. When the concrete is crushed, the compression steel bar has achieved the yield strength or very close to the yield strength. The ductility of large eccentric steel tube-reinforced concrete column structure is better than that of small eccentric steel tube-reinforced concrete column structure, but the ultimate bearing capacity decreases with increasing of the eccentricity. Li *et al*. (1999) discussed the failure modes, deformation capacity, energy dissipation and strain distribution of high strength steel tube-reinforced concrete column structure, analyzed the distribution of axial force between concrete and steel tube, and proposed the design formula for the nominal axial compression ratio. After the yielding of steel stirrups in outer concrete, the steel strip can serve as a role of "secondary stirrups" and restrain the concrete (Skalomenos *et al*. 2015). Cao *et al*. (Cao *et al*. 2013) studied the seismic behaviors of rectangular steel tube-reinforced concrete column structure with bottom strengthened, and proposed the corresponding design formulas.

Recently, due to high calculation efficiency and accuracy, the finite element method has been widely used in the analysis of steel tube-reinforced concrete column structure. There are a growing number of references on the numerical calculation of steel tube-reinforced concrete column structure. Li and Liao (2013) found that the ultimate bearing capacity of CFSTRC decreases and the deflection increases under long-term sustained loading. Wu *et al*. (2014) studied the effect of preload on the axial bearing capacity of steel tube-reinforced concrete column structure and discussed the effects of cross section, steel grade and concrete grade (Neuenschwander *et al*. 2016, 2017).

The current researches are mainly on the seismic performances of steel tube-reinforced concrete column structure, and there are few references on the mechanical properties of beam-column joints. For ring beam joints, the ring beam can release the stress concentration in the core area, compared with bar reinforced joints, but also changes the stress distributions of core area (Kara *et al*. 2015). Besides, the concrete grade, steel tube grade and reinforcement ratio may affect the failure mode and ultimate bearing capacity of steel tube-reinforced concrete

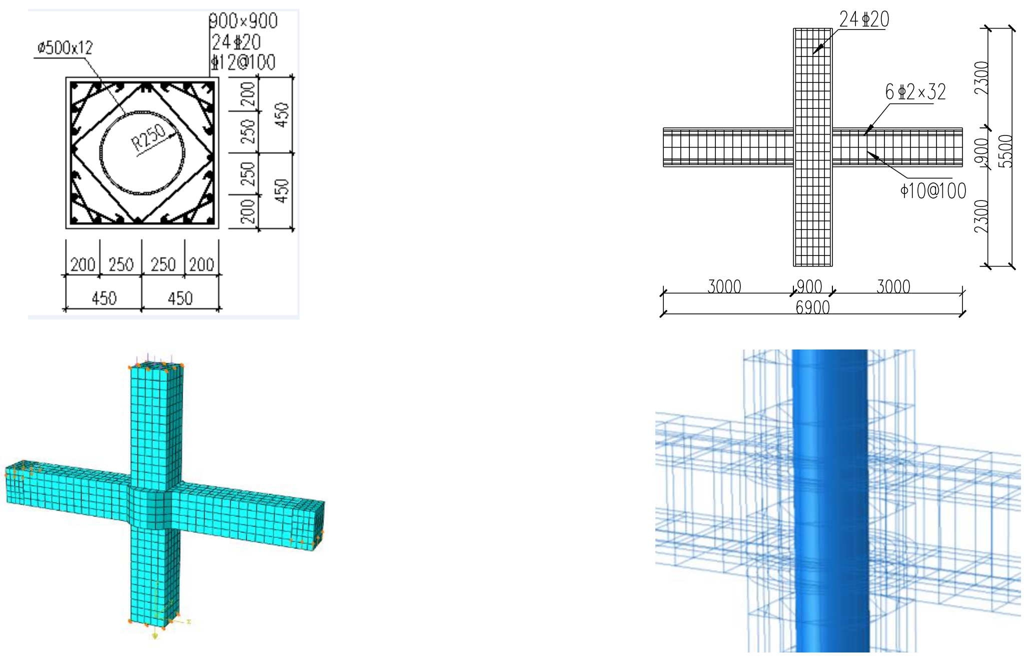

Fig. 2 Numerical model and dimensions of steel tube-reinforced concrete column structure joints

Table 1 Details of specimens

Specimens Number	Concrete	Steel tube	Radius-to-width ratio	Reinforcement ratio
STRCH1	C60	Q235	2	0.75
STRCH2			2	1.25
STRCH3			3	0.75
STRCH4			3	1.25
STRCH5		Q345	2	0.75
STRCH6			2	1.25
STRCH7			3	0.75
STRCH8			3	1.25
STRCH9	C80	Q235	2	0.75
STRCH10			2	1.25
STRCH11			3	0.75
STRCH12			3	1.25
STRCH13		Q345	2	0.75
STRCH14			2	1.25
STRCH15			3	0.75
STRCH16			3	1.25

column structure joints. Nie *et al*. (2012) carried out the tests on the seismic behaviors of outer stiffening ring joints, and proposed some constructional methods. Therefore, it is necessary to study the failure modes and ultimate capacity of ring beams joints (Shakir *et al*. 2016).

The ring beam joints in Shanghai Xinghui Center is taken as the research object. First, the finite element models are built to simulate the seismic behaviors of ring beams of steel tube-reinforced concrete column structure joints (Mollazadeh and Wang 2016). Then, the effects of concrete grade, steel tube grade, reinforcement ratio, and reinforcement distribution on seismic behaviors of ring beam joints are studied (Jeddi *et al*. 2016). Finally, the storing force model is proposed to describe the seismic behaviors of ring beams joints. This paper can provide a good reference for the seismic behaviors of steel tube-reinforced concrete column structure joints (Kwan *et al*. 2016).

2. Materials and methodology

The finite element method is used to analyze the steel tube-reinforced concrete column structure joints. For steel tube, the perfect elastic-plastic relation is used. For concrete, there are two types of constitutive relations, regarding to the outer and core concrete of steel tube-reinforced concrete column structure (Dong *et al*. 2017). For outer concrete, the damage plastic model is used, according to the current design codes (MOHURD 2010).

The ring beams of connections in Shanghai Xinghui Center is taken as the research object. There are 16 specimens and the details are shown in Fig. 2 and Table 1. All the specimens have the same dimension. The column is with the cross section of 900 mm × 900 mm and the height of 5.5 m. The beam is with the cross section of 800 mm × 900 mm and the length of 6 m. The steel tube is with the outer diameter of 512 mm and the thickness of 12 mm. All the reinforcements are HRB400 and all the stirrups are HPB300. For column, the longitudinal reinforcements are $24\phi25$ and the stirrups are $\phi12@100$. For the beam, the upper and bottom reinforcements are $6\phi2 \times 32$, and the stirrup is $\phi10@100$.

The tangent behavior between steel tube and concrete is defined as the penalty contact, and the friction coefficient is 0.3. The normal behavior is defined as the hard contact, in which the steel tube is the main surface and the concrete is the slave surface. The slip effect between steel and concrete is neglected, and the embedded contact is conducted. The column ends are fixed by hinge joint. The axial force is applied in the column top and the axial compression ratio is 0.3. The loading protocol is controlled by displacement, every increment is 10 mm and two cycles in one level. The gasket with infinite stiffness is applied in the column top, in order to avoid the local crushing of concrete.

The mass density of concrete is 2.4×10^3 kg/m^3, and the elastic modulus are 3.25×10^4 MPa (C40), 3.6×10^4 MPa (C60), and 3.8×10^4 MPa (C80), respectively. The boundary conditions are the same as the referenced tests. The steel gaskets are set in the column ends and the hinge conditions are used. The loading protocol is controlled by displacement. The displacement increment of each level is 2 mm and twice in one increment (MOHURD 2015).

3. Results and discussions

3.1 Verification of numerical calculation method

The finite element analysis is conduced to simulate the tests in Reference (Qian and Jiang 2009), in order to verify the accuracy of numerical analysis method. The dimensions and material properties of specimens are the same as the tests. Three groups of specimens are named as "CCS1, CCS2 and CCS3". The compressive strength of concrete in the beam is 30.1 MPa, respectively. The compressive strength of concrete in the column and ring beam is 53.53 MPa. For concrete, the elastic modulus and Poisson ratio is 3.6×10^4 MPa and 0.2. For steel, the elastic modulus and Poisson ratio is 2.06×10^5 MPa and 0.3, the yield strength of the steel tube is 345 MPa and the mass density is 7.8 g/cm^3. The elements for concrete and steel are C3D8R and C3D8I. The longitudinal reinforcements in beam and column are HRB 400, the stirrups are HRB 335 and the bar element is truss element.

Table 2 shows the comparisons between numerical calculations and experiment data in Qian's reference (Lee and Fenves 1998). Where, F_y, Δ_y, θ_y are the yielding load, displacement and rotation angle. Where, F_m, Δ_m, θ_m are the peak load, displacement and rotation angle, and F_u, Δ_u, θ_u are the failure load, displacement and rotation angle. 85% of the peak load is taken as the ultimate load. It can be observed that the peak load of the numerical calculation is about 10% higher than experiment data. This may be because in the experiment, the concrete strength may not achieve the design strength, due to lack of enough vibration

Table 2 Comparisons between numerical simulation and experiment data of steel tube-reinforced concrete column structure specimens

Referenced specimen	Yielding point			Peak point			Ultimate point		
	F_y (kN)	Δ_y (mm)	θ_y	F_m (kN)	Δ_m (mm)	θ_m	F_u (kN)	Δ_u (mm)	θ_u
Numerical simulation	129	12.3	1/128	177.2	23.2	1/68	129.5	54	1/29
Experiment data	123	11.8	1/134	184	23.5	1/67	125	52.7	1/30

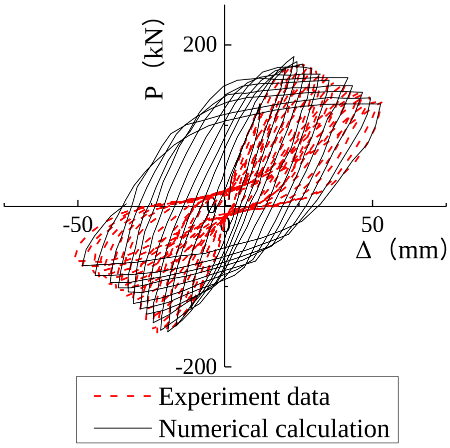

Fig. 3 P-Δ hysteresis curves of specimens

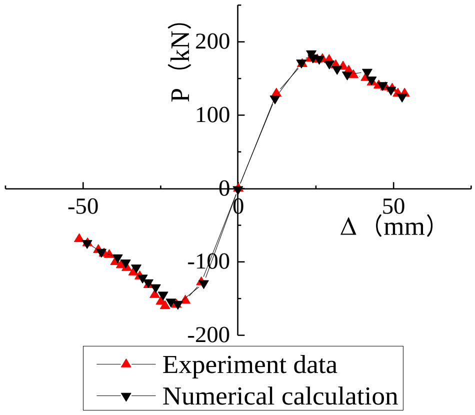

Fig. 4 Skeleton curves of specimens

in the concrete pouring. As shown in Fig. 3, the hysteretic curve of numerical calculation looks better than the test curves. The skeleton curves of three specimens are shown in Fig. 4. Besides, ignoring of bar slip may also lead to the slight differences between experiment data and numerical calculation (Nie *et al*. 2012). This is mainly because that after the cracking of outer concrete, the reinforcement yields fast because of ignoring the slip between bar and concrete. From the hysteretic curves and skeleton curves, increasing the stirrup can improve the energy dissipation ability. The numerical calculation is consistent with the

Table 3 Numerical simulations ring beam joints of steel tube-reinforced concrete column structure

Specimen number	Concrete	Steel	Radius-to width ratio	Reinforcement ratio	Yield phase			Peaking phase			Ultimate phase		
					F_y (kN)	Δ_y (mm)	θ_y	F_m (kN)	Δ_m (mm)	θ_m	F_u (kN)	Δ_u (mm)	θ_u
STRCH1	C60	Q235	2	0.75	618	8	1/375	739	12	1/250	702	36	1/83
STRCH2			2	1.25	614	8	1/375	732	12	1/250	679	36	1/83
STRCH3			3	0.75	616	8	1/375	701	12	1/250	668	32	1/94
STRCH4			3	1.25	614	8	1/375	723	12	1/250	619	40	1/75
STRCH5		Q345	2	0.75	618	8	1/375	739	12	1/250	682	40	1/75
STRCH6			2	1.25	615	8	1/375	733	12	1/250	689	40	1/75
STRCH7			3	0.75	616	8	1/375	702	12	1/250	683	36	1/83
STRCH8			3	1.25	614	8	1/375	723	12	1/250	661	36	1/83
STRCH9	C80	Q235	2	0.75	618	6	1/500	821	16	1/188	698	40	1/75
STRCH10			2	1.25	619	6	1/500	804	16	1/188	683	40	1/75
STRCH11			3	0.75	614	6	1/500	763	14	1/214	522	34	1/88
STRCH12			3	1.25	615	6	1/500	788	16	1/188	670	40	1/75
STRCH13		Q345	2	0.75	619	6	1/500	822	16	1/188	699	40	1/75
STRCH14			2	1.25	619	6	1/500	804	16	1/188	683	38	1/79
STRCH15			3	0.75	614	6	1/500	763	14	1/214	522	34	1/88
STRCH16			3	1.25	616	6	1/500	765	14	1/214	650	39	1/77

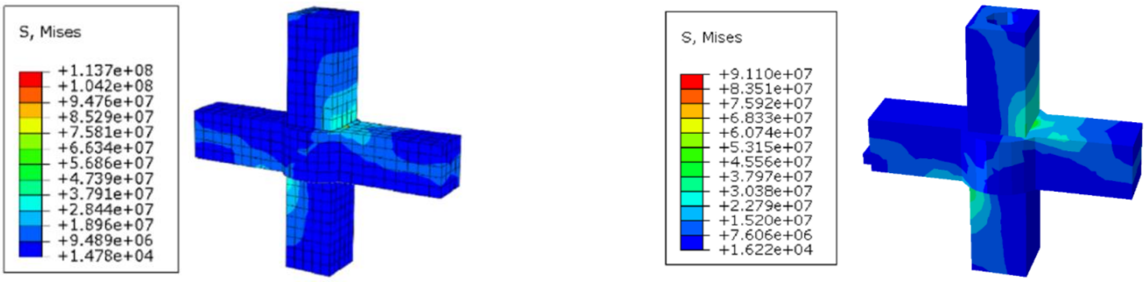

STRCH3 STRCH15

(a) Concrete

STRCH3 STRCH15

(b) Steel tube

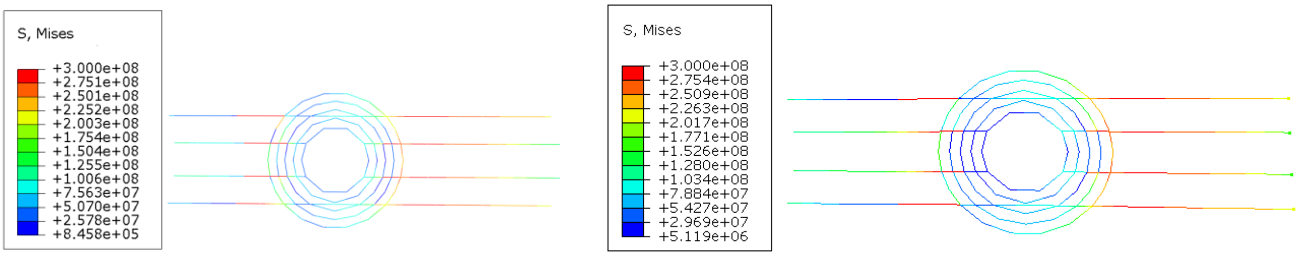

STRCH3 STRCH15

(c) Ring beam

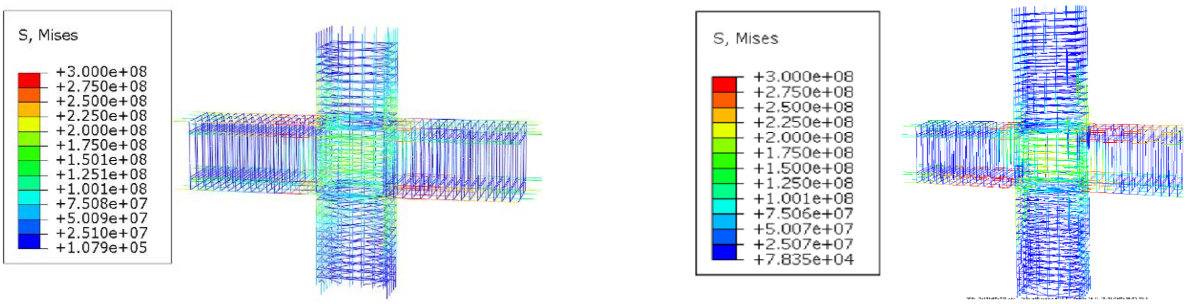

STRCH3 STRCH15

(d) Steel bar

Fig. 5 Failure modes of FEM of specimens

experiment data. The analysis method of numerical calculation can be used to simulate the seismic behaviors of beam-column joints of steel tube-reinforced concrete column structure.

3.2 Numerical simulation of ring beams joints of steel tube-reinforced concrete column structure

This part mainly presents the hysteretic behaviors of ring beams joints of steel tube-reinforced concrete column structure under cyclic loading. To compare better, the yielding load F_y and the yielding displacement Δ_y of the specimen are determined based on the skeleton curve using the graphical method. The peak load F_m corresponds to the maximum value of the beam end load on the skeleton curve, and the peak displacement Δ_m is the displacement value corresponding to the peak load. For the ultimate load, when the load can decrease to 85% of the peak load, 85% of the peak load is considered to as the ultimate load. If the load cannot decrease to 85% of the peak load, the final load of the calculation is taken as the ultimate load. The numerical calculations of ring beams joints are shown in Table 3. It can be found that when the radius-to-width ratio is 2, increasing the reinforcement ratio will reduce the ultimate bearing capacity of specimens. When the radius-to-width ratio is 3, the increasing of reinforcement ratio will improve ultimate bearing capacity of specimens. For the specimens STRCH1 and STRCH3 (STRCH5 and STRCH7, STRCH9 and STRCH11, STRCH13 and STRCH15), the ultimate bearing capacity decreases with the radius-to-width ratio increasing. Besides, the grade of steel tube has no effects on the peak load of specimens, and enhancing the grade of concrete can improve the ultimate capacity of specimens effectively (Clough 1966).

3.3 Failure modes

Fig. 5 shows the failure modes and stress distributions of the specimens. Fig. 6 shows the principle plastic strain vectors of concrete. The appearance of principal tensile plastic strain means the cracking of concrete and the orientation of crack is perpendicular to the principal tensile plastic strain.

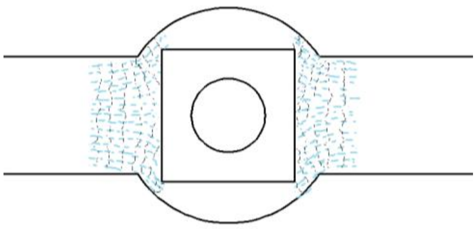

Fig. 6 Principle plastic strain vectors of concrete

As shown in Fig. 5(a), when the connection fails, the failure appears at the ring beam and the beam end. As shown in Fig. 5(b), when the connection fail, the stress of the steel tube is far lower than the yielding stress. Changing the grade of steel tube has little effect on the bearing capacity of the joint. As shown in Fig. 5(c), when the joint fails, the longitudinal bars in the beam and ring beam achieve the yielding strength, indicating that the ring beam joint can effectively transfer the moment and the force. As shown in Fig. 5(d), when the joint fails, the maximum stress of the steel bar appears in ring beam and concrete beam. It can be concluded that the ring beam can absorb enough energy, in order to avoid the crushing of core concrete, which can satisfy the seismic requirements. From above, for all specimens, it can be found that the failure of joints under low cyclic loading appears at the ring beam and beam end. The differences among them are that with the changing of reinforcement ratio, the stress distributions of ring beam and frame beam change, which leads to the changing of crack distribution in the concrete (Wang and Shao *et al*. 2017).

3.4 Hysteretic curves and skeleton curves

The hysteretic curves and skeleton curves are shown in Figs. 7 and 8. It can be seen that the load-displacement curves perform good energy dissipation ability and ductility. There are four phases in the skeleton curves, including elastic, elastic-plastic, plastic and failure. It is a typical ductile failure mode. It proves that the ring beam joint can be a good pass to transmit power from the beam to the joint.

From the skeleton curves and Table 3, it can be seen that

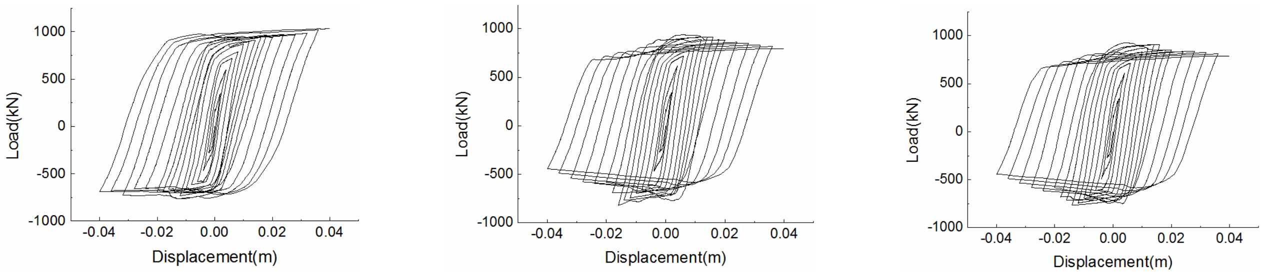

(a) STRCH2 (b) STRCH9 (c) STRCH15

Fig 7 Hysteresis curves of specimens

(a) The radius-to-width ratio is 2, The reinforcement ratio is1.25, Steel grade is Q235

(b) The radius-to-width ratio is 2, The reinforcement ratio is0.75, Steel grade is Q345

Fig. 8 Skeleton curves of ring-beam joints

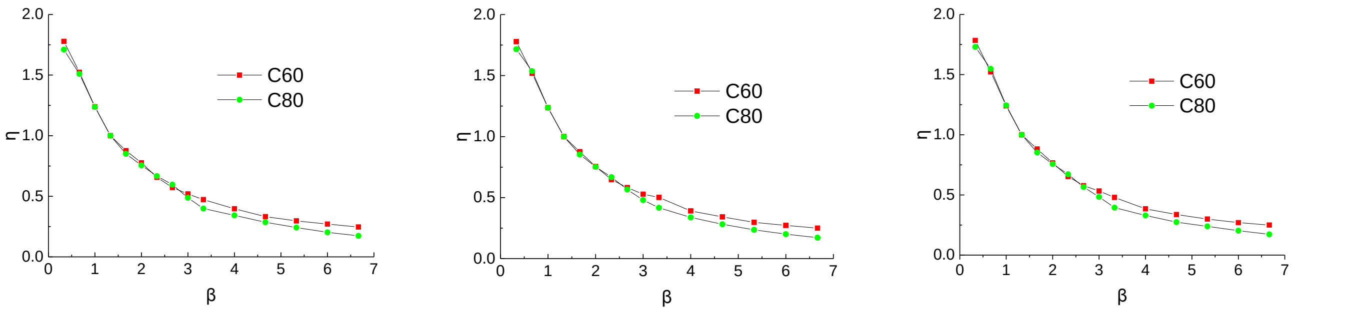

(a) The radius-to-width ratio is 2, The reinforcement ratio is 1.25, Steel grade is Q345

(b) The radius-to-width ratio is 3, The reinforcement ratio is 0.75, Steel grade is Q235

(c) The radius-to-width ratio is 3, The reinforcement ratio is 1.25, Steel grade is Q345

Fig. 9 Stiffness degradation curves of ring-beam joints

radius-to-width ratio, reinforcement ratio and concrete strength have some effects on the ultimate bearing capacity of specimens. From Table 3, it can be seen that increasing the concrete strength can significantly improve the bearing capacity of specimens under low cycle loading. When the concrete grade increases from C40 to C60 or C60 to C80, the peak load increased about 15%. The effect of the grade of steel tube on the ultimate bearing capacity of specimens is not significant. This is because that when the ring beams joints fail, the steel tube has not achieve the yield strength. It can also be seen from that when the radius-to-width ratio is 2, increasing the reinforcement ratio will reduce the ultimate bearing capacity of specimens. When the radius-to-width ratio is 3, increasing the reinforcement ratio can increase the ultimate bearing capacity of specimens. Increasing the radius-to-width ratio will result in a slight decrease of the ultimate bearing capacity of specimens.

This is because with the increasing of the radius-to-width ratio, the reinforcement ratio at the core of the ring beam decreased and the contribution of concrete reduced. Then, the concrete is easy to be crushed under repeated loading, resulting in the decrease of the ultimate bearing capacity of specimens. The reinforcement ratio affects the distribution ratio between ring beam and frame beam. When the radius-to-width ratio is relatively small, the ultimate bearing capacity of ring beam is higher than the frame beam. Increasing the reinforcement ratio will lead to the crush of beam concrete more easily. Then, the steel bars of ring beam do not achieve the yield strength, so the ultimate bearing capacity of specimens decreases. When the radius-to-width ratio is relatively large, the ultimate bearing capacity of frame beam is higher than the ring beam. Increasing the reinforcement ratio will reduce the load of the ring beam, which may lead to the failure of ring beam and frame beam concrete at the same time. Then, the ultimate bearing capacity increases.

3.5 Stiffness degradation and energy dissipation ability

In order to study the stiffness degradations, the secant stiffness of specimens under cyclic loading can be calculated. Fig. 9 shows the degradation curves of specimens. Where, β is the ratio of Δ_i (the peak displacement in the cycle i) and Δ_y (the yield displacement), η is the ratio of K_i (the secant stiffness in the loading level i) and K_y (the secant stiffness at the yield point). As shown in Fig. 9, significant stiffness degradation can be observed under cyclic loading. Various factors have little effect on the stiffness degradation rate of specimens. Changing the grade of steel tube has no effect on the stiffness degradation of specimens. Increasing the concrete grade can slightly enhance the degradation rate of structural stiffness. With the increase of radius-to-width ratio, the stiffness degradation rate of the specimen is slightly increased. The effect of reinforcement ratio on the stiffness degradation rate is slight.

Under cyclic loading, the specimens absorb energy in the loading process and release energy in the unloading process. As shown in Fig. 10, the absorb energy in the loading process of every cycle is the area of OABC. The released energy in the unloading process is the area of BCD. The area of OABD, the difference between OABC and BCD, is the energy dissipation during this cycle. It can be obtained by integrating the hysteresis loop.

Table 4 shows the energy dissipation results of specimens under cyclic loading. It can be seen that with cycle number increasing, the specimens perform good energy dissipation ability. Increasing the strength of steel tube steel will slightly increase the energy consumption of the specimen by an increase of less than 1%.When the concrete grade increases from C60 to C80, the cumulative energy consumption of the component increases by about 3%. With radius-to-width ratio increasing, the energy dissipation ability of specimens increases about 1%. When the concrete grade is C60, the cumulative energy consumption of the specimen decreases slightly as the

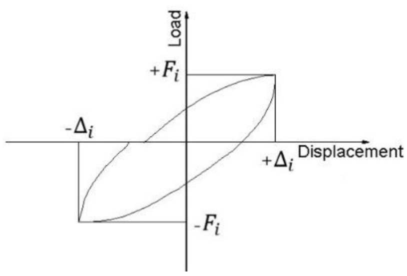

Fig. 10 Energy calculation

Table 4 Energy consumption of specimens

Specimen number	STRCH1	STRCH2	STRCH3	STRCH4	STRCH5	STRCH6	STRCH7	STRCH8
Energy dissipation (kN·m)	414.051	413.734	417.211	415.641	414.490	414.045	418.886	417.522
Increment	0	-0.08%	0	-0.37%	0	-0.11%	0	-0.32%
Specimen number	STRCH19	STRCH10	STRCH11	STRCH12	STRCH13	STRCH14	STRCH15	STRCH16
Energy dissipation (kN·m)	425.143	430.433	426.977	430.383	424.530	429.772	427.250	430.940
Increment	0	+1.24%	0	+0.79%	0	+1.23%	0	+0.86%

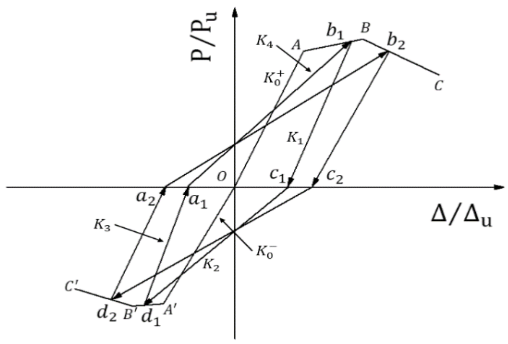

Fig. 11 Tri-linear model considering stiffness degradation

reinforcement ratio increases. When the concrete is C80, as the reinforcement ratio increases, the cumulative energy dissipation of specimens increases slightly.

3.6 Restoring force model

The tri-linear restoring force model is conducted to describe the restoring force characteristics of ring beams joints of steel tube-reinforced concrete column structure, as shown in Fig. 11. It can consider the stiffness degradation and is suitable for the seismic analysis of steel tube-reinforced concrete column structure. The dimensionless method is used to reduce the effect of experimental parameters on the restoring force model. Where, the vertical ordinate is the ratio of the load P to the peak load P_u, The horizontal ordinate is the ratio of displacement Δ to peak displacement Δ_u. A and A' are the yield points. OA and $O'A'$ are the skeleton curve of the elastic phase. Respectively from the initial curve of the skeleton yield point regression data obtained, the slope of the node that the initial stiffness. B and B' are the peak load points. AB and $A'B'$ are the elastic-plastic phases of the skeleton curve, which are obtained from the initial yield point data and the peak load point data. The slope represents the plastic stiffness after yielding. C and C' are the failure points. BC and $B'C'$ are the descending sections of the skeleton curve, and are obtained by regression of peak load point data and failure point data.

All the dimensionless skeleton curves were analyzed by regression analysis, as shown in Fig. 12. All the segments In Fig. 11 can be obtained by the data in Fig. 12. The regression equation for each segment is shown in Eq. (1).

$$P / P_u = k \cdot \Delta / \Delta_u + b \quad (1)$$

From the numerical calculations, the stiffness degradation can be observed for the ring beams joints of steel tube-reinforced concrete column structure under low cyclic loading. In order to study the restoring force model, the

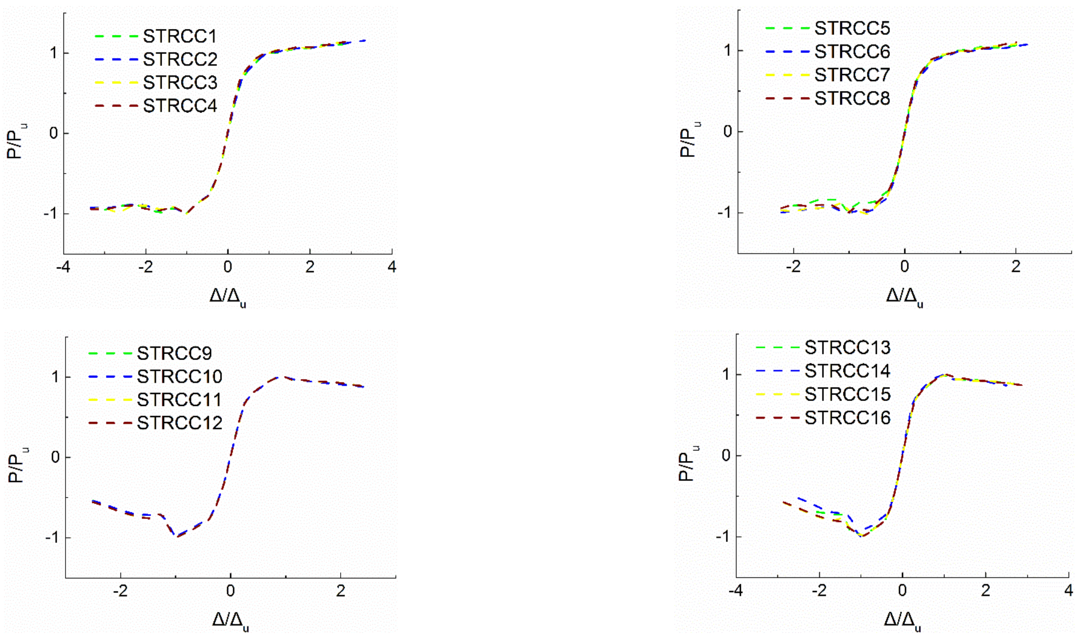

Fig. 12 Non-dimensional skeleton curves of ring beams joints

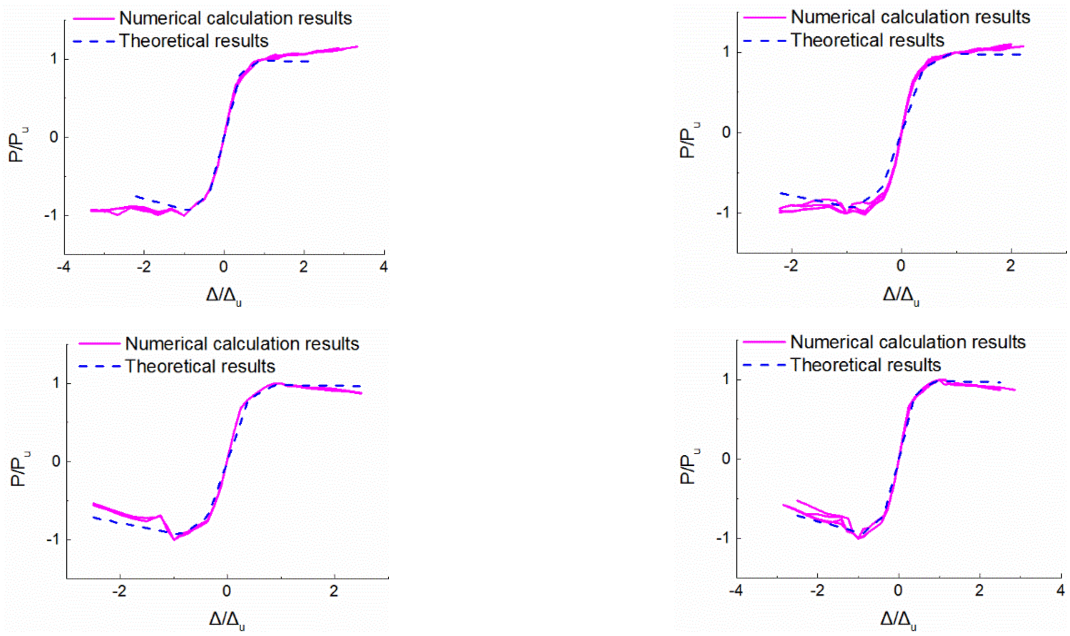

Fig. 13 Comparisons between model predictions and numerical simulations for ring beams joints

degradation law of loading stiffness and unloading stiffness of joints under low cyclic loading can be obtained first. Where, K_0 is the initial stiffness of the specimen, K_1 is the forward unloading stiffness, K_2 is the reverse loading stiffness, K_3 is the reverse unloading stiffness and K_4 is the forward loading stiffness.

The degradation of forward unloading stiffness K_1 can be described as

$$K_1/K_0^+ = -0.149ln(\Delta_1/\Delta_0^+) + 0.566 \tag{2}$$

The degradation of reverse loading stiffness K_2 can be expressed as

$$K_2/K_0^- = 0.783e^{-0.706(\Delta_1'/\Delta_0^+)} \tag{3}$$

The degradation of reverse unloading stiffness K_3 can be expressed as

$$K_3/K_0^- = -0.131ln(\Delta_2/\Delta_0^-) + 0.571 \tag{4}$$

The degradation of forward loading stiffness K_4 can be expressed as

$$K_4/K_0^+ = 0.728e^{-0.624(\Delta_2'/\Delta_0^-)} \tag{5}$$

Fig. 13 shows the comparisons between the predictions of restoring force models and numerical calculations. The storing force model can make a good prediction of yielding points, peak points, ultimate points and load-displacement curves. The simplified tri-linear curves agree well with the numerical skeleton curves. The reason why the two ends of the skeleton curve have a slight difference is mainly due to the slip between the concrete and the steel pipe under the repeated low-cycle load. From above, the proposed restoring force model for the steel tube-reinforced concrete column structure specimens is reliable and can be used for the seismic analysis (Kasar and Bharti *et al*. 2017; Prashob and Shashikala *et al*. 2017).

4. Conclusions

This paper presents the seismic behaviors and restoring force model of ring beam joints of steel tube-reinforced concrete column structure. The effects of concrete grade, steel tube grade, reinforcement ratio, radius to width ratio on the seismic behaviors of steel tube-reinforced concrete column structure connections are studied. The following conclusions can be obtained.

- For the ring beams joints of steel tube-reinforced concrete column structure, the failure under cyclic loading appears at the connection between ring beam and frame beam. The concrete at the ring beam and the end of frame beam is crushed, in which some bars have achieved the yield strength. The steel tube and the laminated column concrete is far lower than the yield stress. It can be seen that the failure mode of ring beam joint conform to the design concept of “strong column and weak beam”.
- For the ring beams joints of steel tube-reinforced concrete column structure, increasing the grade of concrete can improve the ultimate bearing capacity and energy dissipation ability of specimens, but will slightly increase the degradation rate of structural stiffness. Increasing the grade of steel tube can only slightly increase the energy dissipation ability of specimens, but has no effects on the ultimate bearing capacity and stiffness degradation rate. Changing the reinforcement ratio can change the final distribution of cracks. When the radius-to-width ratio is relatively small, increasing the reinforcement ratio will reduce the ultimate bearing capacity of

specimens. When the radius-to-width ratio is relatively large, the reinforcement ratio will increase the ultimate bearing capacity of specimens, but has no effects on the stiffness degradation and energy dissipation ability. Increasing the radius-to-width ratio will lead to a slight decrease of the ultimate bearing capacity of specimens and a slight increase of stiffness degradation rate and energy dissipation ability.

The dimensionless method is used to reduce the effect of concrete strength and steel strength on the restoring force characteristics of joints. The tri-linear restoring force model of bar reinforced steel tube-reinforced concrete column structure joints can be obtained based on the skeleton curves. The predictions of the restoring force model agree well with the numerical simulations. It can provide good references for the seismic analysis of similar joints.

Acknowledgments

The research described in this paper was financially supported by National Key Research and Development Plan, China (2017YFC1500700).

Conflict interests

The authors declare that they have no conflict of interests regarding the publication of this paper.

References

Cao, W., Hui, C., Dong, H., Xu, F. and Qiao, Q. (2013), "Study on seismic behavior of bottom strengthened rectangular steel tube reinforced concrete columns", *World Earthq. Eng.*, **29**(3), 14-19.

CECS (2005), Technical specification for steel tube-reinforced concrete column structure, China Planning Press, Beijing, China.

Clough, R.W. (1966), *Effect of Stiffness Degradation on Earthquake Ductility Requirements*, University of California.

Dong, C.X., Kwan, A.K.H. and Ho, J.C.M. (2017), "Effects of external confinement on structural performance of concrete-filled steel tubes", *J. Const. Steel Res.*, **132**, 72-82.

Jeddi, M.Z., Sulong, N.H.R. and Khanouki, M.M.A. (2016), "Seismic performance of a new through rib stiffener beam connection to concrete-filled steel tubular columns: An experimental study", *Eng. Struct.*, **131**(15), 477-491.

Kara, I.F., Ashour, A.F. and Köroğlu, M.A. (2015), "Flexural behavior of hybrid FRP/steel reinforced concrete beams", *Compos. Struct.*, **129**, 111-121.

Kasar, A.A., Bharti, S.D., Shrimali, M.K. and Goswami, R. (2017), "Mechanics based force-deformation curve of steel beam to column moment joints", *Steel Compos. Struct., Int. J.*, **25**(1), 19-34.

Kwan, A.K.H., Dong, C.X. and Ho, J.C.M. (2016), "Axial and lateral stress-strain model for circular concrete-filled steel tubes with external steel confinement", *Eng. Struct.*, **117**(15), 528-541.

Li, Y. and Liao, F. (2013), "Behaviour of Concrete Filled Steel Tube Reinforced Concrete Columns Subjected to Long-term Sustained Loading", *J. Beijing Univ. Technol.*, **36**(2), 79-86.

Li, H., Wang, Z. and Wu, B. (1999), "Analysis on Axial Loading Distribution and Limitation of Nominal Axial Compression Ratio of Laminated Column With High Strength Concrete Filled Steel Tube", *World Info. Earthq. Eng.*, **15**(2), 1-8.

Lee, J. and Fenves, G.L. (1998), "Plastic-Damage Model for Cyclic Loading of Concrete Structures", *J. Eng. Mech.*, **124**(8), 892-900.

MOHURD (2010), Code for design of concrete structures; Beijing, China.

MOHURD (2015), Specification for seismic test of building; China Architecture & Building Press, Beijing, China.

Mollazadeh, M.H. and Wang, Y.C. (2016), "New Mechanism of Load Introduction into Concrete-Filled Steel Tubular Columns", *J. Struct. Eng.*, **142**(6), 4016016.

Neuenschwander, M., Knobloch, M. and Fontana, M. (2016), "ISO Standard Fire Tests of Concrete-Filled Steel Tube Columns with Solid Steel Core", *J. Struct. Eng.*, **143**(4), 4016211.

Neuenschwander, M., Knobloch, M. and Fontana, M. (2017), "Modeling thermo-mechanical behavior of concrete-filled steel tube columns with solid steel core subjected to fire", *Eng. Struct.*, **136**(1), 180-193.

Nie, J. (2011), *Composite Structures of Steel and Concrete: Theory and Practice*, Architecture &Building Press, Beijing, China.

Nie, J., Wang, Y. and Fan, J. (2012), "Experimental study on seismic behavior of concrete filled steel tube columns under pure torsion and compression-torsion cyclic load", *J. Constr. Steel Res.*, **79**(1), 115-126.

Prashob, P.S., Shashikala, A.P. and Somasundaran, T.P. (2017), "Behaviour of carbon fiber reinforced polymer strengthened tubular joints", *Steel Compos. Struct., Int. J.*, **24**(4), 383-390.

Qian, J. and Jiang, Y. (2009), "Tests on seismic behavior of RC beam-composite steel tube confined concrete column joints", *Build. Struct.*, **39**(9), 39-42.

Shakir, A.S., Guan, Z.W. and Jones, S.W. (2016), "Lateral impact response of the concrete filled steel tube columns with and without CFRP strengthening", *Eng. Struct.*, **116**, 148-162.

Skalomenos, K.A., Hatzigeorgiou, G.D. and Beskos, D.E. (2015), "Modeling level selection for seismic analysis of concrete-filled steel tube/moment-resisting frames by using fragility curves", *Earthq. Eng. Struct. Dyn.*, **44**(2), 199-220.

Wang, W., Tang, Z., Li, Z. and Ma, H. (2016), "Bearing Capacities of Different-Diameter Concrete-Filled Steel Tubes under Axial Compression", *Adv. Mater. Sci. Eng.*, **2016**(473), 1-10.

Wang, Y., Shao, Y., Song, S. and Yang, D. (2017), "Static test on failure process of tubular T-joints with initial fatigue crack", *Steel Compos. Struct., Int. J.*, **24**(5), 615-633.

Wu, X.U., Qing, Y.U. and Guohuang, Y.A.O. (2014), "Effect of preload on the axial capacity of CFST reinforced concrete columns", *J. Tsinghua Univ.*, **54**(5), 556-562.

Yu, M., Zha, X., Ye, J. and Li, Y. (2013), "A unified formulation for circle and polygon concrete-filled steel tube columns under axial compression", *Eng. Struct.*, **49**(2), 1-10.

Zhong, S. (2003), *The Concrete-Filled Steel Tube Structures*, Tsinghua University Press, Beijing, China.

CC